Chaos, Solitons and Fractals 181 (2024) 114650

Contents lists available at ScienceDirect

Chaos, Solitons and Fractals

journal homepage: www.elsevier.com/locate/chaos

*n*D-CS: A circularly shifting chaotic map generation method

Zihua Wu [a], Yinxing Zhang [a], Han Bao [b], Rushi Lan [c], Zhongyun Hua [a,*]

[a] School of Computer Science and Technology, Harbin Institute of Technology, Shenzhen, Guangdong, 518055, China
[b] School of Microelectronics and Control Engineering, Changzhou University, Changzhou, 213164, China
[c] Guangxi Key Laboratory of Image and Graphic Intelligent Processing, Guilin University of Electronic Technology, Guilin, 541004, China

ARTICLE INFO

Keywords:
Chaotic map generation
High-dimensional chaotic map
Hyperchaotic behavior
Lyapunov exponent

ABSTRACT

Due to more complex behavior and larger number of control parameters, high-dimensional chaotic map generation methods may provide more satisfactory performance in various practical applications compared to low-dimensional counterparts. Designing *n*-dimensional (*n*D) chaotic map generation methods for generating chaotic maps in arbitrary dimensions with desired dynamics is an interesting but challenging task. In this paper, we propose a universal framework called the *n*D circularly shifting chaotic map generation method (*n*D-CS), which utilizes existing one-dimensional chaotic maps as seed maps to generate *n*D chaotic maps with complex and robust behaviors. Theoretical analysis proves that when specific criteria are met by its control parameters, our *n*D-CS can exhibit complex and robust hyperchaotic behavior in the sense of Lyapunov exponent. To demonstrate the effectiveness of our *n*D-CS, we first employ it to generate three examples of three-dimensional hyperchaotic maps. The results indicate high-performance indicators of these new chaotic maps. Furthermore, we compare the *n*D chaotic maps generated by our *n*D-CS to those produced by existing methods. The results demonstrate that our chaotic maps have a better overall performance.

1. Introduction

Chaos is a phenomenon that shows complex and ostensible irregular behavior [1], often referred to as the butterfly effect. It is commonly observed in initial-sensitive dynamic systems, where even small disturbances in initial states can result in significantly different outcomes as time progresses [2]. Consequently, chaos theory has been developed to explore various natural and man-made phenomena that exhibit chaotic behaviors, such as weather forecasting [3], fluid dynamics [4], population growth [5], and financial markets [6]. Chaotic maps, which are discrete nonlinear mathematical models used to study chaotic behaviors [7], possess several distinctive characteristics, including initial state sensitivity, unpredictability, ergodicity, and parameter controllability [8,9]. The initial state sensitivity implies that even minor deviations from the initial states can lead to substantially different behaviors. Unpredictability refers to the inability to accurately predict long-term behavior. Ergodicity indicates that every state in the phase space has the opportunity of being accessed. Parameter controllability signifies that the exhibited behaviors are influenced by parameters, and different parameter settings enable diverse behaviors. These characteristics make chaotic maps compelling candidates for various practical applications [10,11], including image encryption [12], secure communication [13], and pseudo-random number generation [14].

Chaotic maps can be classified into two categories based on their dimensionality: low-dimensional chaotic maps and high-dimensional chaotic maps. In general, low-dimensional chaotic maps possess simple structures and low complexity [15,16]. For example, the classical one-dimensional (1D) logistic chaotic map [17], formed by multiplying a quadratic function with a single control parameter, has been extensively utilized in applications like image encryption and pseudo-random number generation [18,19]. In more recent studies, Talhaoui et al. [20] introduced a 1D cosine fractional chaotic map with favorable cryptography properties and high sensitivity to initial conditions. Additionally, Xu et al. [21] proposed a two-dimensional sine improved logistic iterative chaotic map capable of exhibiting hyperchaotic behavior and a high level of randomness. However, many low-dimensional chaotic maps exhibit limitations, such as narrow and discontinuous chaotic intervals, the easy occurrence of chaos degradation, and relatively simple and unstable chaotic behaviors [22,23]. These deficiencies make the generated chaotic sequences easy to predict, thereby impacting the performance of applications that rely on chaotic maps [24].

In contrast, high-dimensional chaotic maps possess more complex structures along with wider continuous chaotic intervals [25], leading to complex behaviors that yield impressive performance across

* Corresponding author.
E-mail addresses: ozoa91011@gmail.com (Z. Wu), yxzhang23@163.com (Y. Zhang), hanbao@cczu.edu.cn (H. Bao), rslan@guet.edu.cn (R. Lan), huazyum@gmail.com (Z. Hua).

https://doi.org/10.1016/j.chaos.2024.114650
Received 11 December 2023; Received in revised form 19 February 2024; Accepted 21 February 2024
Available online 7 March 2024

various evaluation metrics and applications [26]. Nevertheless, constructing high-dimensional chaotic maps is a more demanding task compared to constructing low-dimensional ones, primarily due to the presence of intricate structures and control parameters. This necessitates a designer with a comprehensive understanding of the underlying mechanisms and mathematical principles of chaotic maps. In general, there are two approaches to constructing high-dimensional chaotic maps. The first approach refers to designing high-dimensional chaotic maps with specific dimensions. For example, Sun et al. [27] developed a new six-dimensional non-degenerate hyperchaotic map with six positive Lyapunov exponents (LE) to improve the performance of image compression and reconstruction.

Another approach is to design n-dimensional (nD) chaotic map generation methods that can generate chaotic maps of arbitrary dimensions [28,29]. This approach offers users the flexibility to customize their desired chaotic maps according to specific demands. For example, Natiq et al. [30] proposed an nD chaotic map generation method utilizing sinusoidal functions to enhance the nonlinearity of the generated chaotic maps. Simulation results demonstrate its ability to generate chaotic maps with good ergodicity and wide hyperchaotic behavior. Meanwhile, Huang et al. [31] devised a method for generating nD non-degenerate chaotic maps based on a discrete memristor model. The chaotic maps they generated exhibit complex dynamic behaviors, such as state transition phenomena, initial-boosting behaviors, and large LE. While these studies provide valuable insights into designing nD chaotic map generation methods, the performance of the generated chaotic maps heavily depends on empirical parameter tuning and the insights of designers. This reliance does not always guarantee the stable performance of the generated chaotic maps. Furthermore, the validation of their chaotic behaviors is solely based on experiment, lacking concrete theoretical guarantees. Therefore, these limitations underscore the need for developing nD chaotic map generation methods in a more robust manner.

In light of the above, we propose the nD circularly shifting chaotic map generation method (nD-CS), an innovative framework that utilizes $n-1$ existing 1D chaotic maps as seed maps to generate new nD chaotic maps. Within the nD-CS framework, the positions of the seed maps in each dimension form a circularly shifting relationship. The nD-CS is characterized by multiple tunable parameters, enabling users a high degree of flexibility in generating numerous new chaotic maps. This is achieved by selecting different seed maps and adjusting the values of control parameters. Moreover, the hyperchaotic behavior of the nD-CS is validated through formulaic analysis. To demonstrate the effectiveness of the nD-CS framework, we first present three examples of new three-dimensional (3D) chaotic maps generated by nD-CS and evaluate their performance. The results indicate that the generated chaotic maps exhibit stable performance across various evaluation metrics and posses high-performance indicators. Furthermore, we conduct a comparative analysis between the nD chaotic maps generated by our nD-CS and those by previous methods. The results highlight the superior overall performance of our nD-CS. To sum up, we outline the contributions of this paper as follows.

1. We introduce nD-CS as a universal method for generating nD chaotic maps. This method enables the effective generation of a substantial quantity of new chaotic maps with desired dimensions by utilizing existing 1D chaotic maps as seed maps.
2. We theoretically prove that the chaotic maps generated by nD-CS can show hyperchaotic behavior in the sense of LE under a parameter-controlled criterion.
3. We present three examples of 3D chaotic maps generated by nD-CS and elaborately evaluate their performance using various metrics to demonstrate the effectiveness of nD-CS.
4. We conduct a comprehensive comparison between nD-CS and other methods for chaotic map generation. The results demonstrate that the chaotic maps generated by nD-CS possess stable performance and generally outperform those generated by other methods.

The rest of this paper is organized as follows. Section 2 introduces nD-CS and provides a theoretical analysis of its behavior. Section 3 presents three new 3D chaotic maps generated by nD-CS as examples and analyzes their properties. Section 4 evaluates the comprehensive performance of nD-CS and compares it with several representative nD chaotic map generation methods, and Section 5 concludes this paper.

2. nD-CS

This section presents the general form of the proposed nD-CS and provides a theoretical demonstration of its hyperchaotic behavior.

2.1. General Form of nD-CS

The nD-CS is an nD discrete chaotic system, where each dimension consists of a linear function, $n-1$ existing 1D chaotic seed maps, and a modular operation. The mathematical definition of nD-CS is given by

$$\mathbf{x}_{i+1} = \mathbf{G}(\mathbf{x}_i, \mathbb{L}, \mathbb{F}, M), \tag{1}$$

where $\mathbf{x}_i = [x_{1,i}, x_{2,i}, \dots, x_{n,i}]^T \in \mathbb{R}^{n\times 1}$ represents the state vector of nD-CS at the ith observation time, and $\mathbf{G}(\mathbf{x}_i, \mathbb{L}, \mathbb{F}, M)$ is a function that takes the current state $\mathbf{x}_i$ as input and produces the subsequent state $\mathbf{x}_{i+1}$ as output. $\mathbb{L} = \{L_1(\cdot), L_2(\cdot), \dots, L_n(\cdot)\}$ denotes the set of n linear functions, $\mathbb{F} = \{F_1(\cdot), F_2(\cdot), \dots, F_{n-1}(\cdot)\}$ denotes the set of $n-1$ existing 1D seed chaotic maps, and M is a positive integer representing the modulus coefficient. Specifically, the general form of nD-CS in Eq. (1) can be expressed as

$$\begin{cases} x_{1,i+1} = L_1(x_{1,i}) + F_1(x_{2,i}) + \cdots + F_{n-1}(x_{n,i}) \bmod M \\ x_{2,i+1} = F_{n-1}(x_{1,i}) + L_2(x_{2,i}) + \cdots + F_{n-2}(x_{n,i}) \bmod M \\ \quad \vdots \\ x_{n,i+1} = F_1(x_{1,i}) + F_2(x_{2,i}) + \cdots + L_n(x_{n,i}) \bmod M. \end{cases} \tag{2}$$

Table 1 presents the mathematical expressions, derivatives, and typical control parameter values of six well-known 1D chaotic maps. These 1D chaotic maps will serve as seed maps for nD-CS in generating new chaotic maps in the following sections. Besides, for unified representation, each linear function in $\mathbb{L}$ can be expressed as

$$L_k(x) = l_k x, \tag{3}$$

where $k \in \{1, 2, \dots, n\}$ and l_k is the parameter of the kth linear function.

2.2. Proof of Chaos

"Chaos" is an observed phenomenon without a universally accepted definition to describe its existence. Among the various definitions of chaos, LE is a widely accepted and employed method that quantifies the divergence rate between two trajectories evolving from neighboring initial states [37]. A positive LE indicates that the two trajectories starting from neighboring initial states will separate in every time unit and eventually exhibit completely different behaviors. The larger the LE, the more complex the dynamic behaviors of the chaotic map.

In general, a dynamic system with a positive LE and a globally bounded phase space can show chaotic behavior. If the dynamic system has more than one positive LE, it can display hyperchaotic behavior. Therefore, the definition of chaos in the sense of LE is specified as Definition 1 [38].

Definition 1 (*[38]*). A dynamic system can exhibit chaotic behavior in the sense of LE if it satisfies two conditions: (1) its phase space is globally bounded; (2) it has at least one positive LE.

According to Eq. (2), the outputs of nD-CS are globally bounded within $[0, M)^n$, thanks to the modular operation. This implies that the condition (1) of Definition 1 can always be satisfied by nD-CS. To make nD-CS meet the condition (2) of Definition 1, we will gradually deduce the circumstance under which nD-CS possesses at least one positive LE.

Table 1
Six well-known 1D chaotic maps.

Map ID	Chaotic map	Expression (F)	Derivative (f)	Typical parameter value ($\bar{a}$)	Value of $\max(\lvert f\rvert)$ when $a=\bar{a}$ and $x\in[0,1)$
1	Chebyshev map [32]	$x_{i+1}=\cos(a\arccos(x_i))$	$\frac{dx_{i+1}}{dx_i}=a\sin(a\arccos(x_i))/(1-x_i^2)^{1/2}$	$\bar{a}=2$	≈ 4
2	Cubic map [33]	$x_{i+1}=ax_i-x_i^3$	$\frac{dx_{i+1}}{dx_i}=a-3x_i^2$	$\bar{a}=3$	3
3	Fraction map [34]	$x_{i+1}=1/(x_i^2+0.1)-ax_i$	$\frac{dx_{i+1}}{dx_i}=-2x_i/(x_i^2+0.1)^2-a$	$\bar{a}=1$	≈ 21.5396
4	Logistic map [17]	$x_{i+1}=ax_i(1-x_i)$	$\frac{dx_{i+1}}{dx_i}=a(1-2x_i)$	$\bar{a}=4$	4
5	Quadratic map [35]	$x_{i+1}=a-x_i^2$	$\frac{dx_{i+1}}{dx_i}=-2x_i$	$\bar{a}=2$	≈ 2
6	Sine map [36]	$x_{i+1}=a\sin(\pi x_i)$	$\frac{dx_{i+1}}{dx_i}=a\pi\cos(\pi x_i)$	$\bar{a}=1$	π

Let us start with the definition of LE. For an nD dynamic system, it possesses n LEs that can be calculated as [39]

$$\mathrm{LE}_k=\lim_{t\to\infty}\frac{1}{t}\ln(\lambda_k(\mathbf{J}_t)),\tag{4}$$

where $k\in\{1,2,\dots,n\}$, and $\lambda_k(\mathbf{J}_t)$ denotes the kth eigenvalue of the matrix $\mathbf{J}_t$. The matrix $\mathbf{J}_t$ is obtained as the product of the Jacobian matrices of nD-CS from observation time 0 to $t-1$, and $\mathbf{J}_t$ can be expressed as

$$\mathbf{J}_t=\prod_{i=0}^{t-1}\mathbf{J}_{\mathbf{x}_i},\tag{5}$$

where $\mathbf{J}_{\mathbf{x}_i}$ represents the Jacobian matrix of nD-CS at the ith observation time and with the observation state $\mathbf{x}_i$. The Jacobian matrix $\mathbf{J}_{\mathbf{x}_i}$ can be expressed as

$$\begin{aligned}\mathbf{J}_{\mathbf{x}_i}&=\begin{bmatrix}\frac{\partial x_{1,i+1}}{\partial x_{1,i}}|_{\mathbf{x}_i} & \frac{\partial x_{1,i+1}}{\partial x_{2,i}}|_{\mathbf{x}_i} & \cdots & \frac{\partial x_{1,i+1}}{\partial x_{n,i}}|_{\mathbf{x}_i}\\ \frac{\partial x_{2,i+1}}{\partial x_{1,i}}|_{\mathbf{x}_i} & \frac{\partial x_{2,i+1}}{\partial x_{2,i}}|_{\mathbf{x}_i} & \cdots & \frac{\partial x_{2,i+1}}{\partial x_{n,i}}|_{\mathbf{x}_i}\\ \vdots & \vdots & \cdots & \vdots\\ \frac{\partial x_{n,i+1}}{\partial x_{1,i}}|_{\mathbf{x}_i} & \frac{\partial x_{n,i+1}}{\partial x_{2,i}}|_{\mathbf{x}_i} & \cdots & \frac{\partial x_{n,i+1}}{\partial x_{n,i}}|_{\mathbf{x}_i}\end{bmatrix}\\&=\begin{bmatrix}l_1 & f_1(x_{2,i}) & \cdots & f_{n-1}(x_{n,i})\\ f_{n-1}(x_{1,i}) & l_2 & \cdots & f_{n-2}(x_{n,i})\\ \vdots & \vdots & \cdots & \vdots\\ f_1(x_{1,i}) & f_2(x_{2,i}) & \cdots & l_n\end{bmatrix},\end{aligned}\tag{6}$$

where $f_1(\cdot),f_2(\cdot),\dots,f_{n-1}(\cdot)$ are the derivatives of the seed maps in the set $\mathbb{F}$ of nD-CS.

Then, based on the knowledge of linear algebra and matrix analysis, we can get that the eigenvalues $\lambda_1\geq\lambda_2\geq\cdots\geq\lambda_n$ and the singular values $\sigma_1\geq\sigma_2\geq\cdots\geq\sigma_n$ of an nD matrix satisfy that

$$\sigma_1\geq|\lambda_k|\geq\sigma_n,\tag{7}$$

where $k\in\{1,2,\dots,n\}$, and σ_1 and σ_n are the maximum and minimum singular values of the nD matrix, respectively. On this basis, we denote $\sigma_1(\mathbf{J}_t)\geq\sigma_2(\mathbf{J}_t)\geq\cdots\geq\sigma_n(\mathbf{J}_t)$ as the singular values of $\mathbf{J}_t$. Therefore, the n LEs of nD-CS calculated by Eq. (4) satisfy that

$$\mathrm{LE}_k=\lim_{t\to\infty}\frac{1}{t}\ln(|\lambda_k(\mathbf{J}_t)|)\geq\lim_{t\to\infty}\frac{1}{t}\ln(\sigma_n(\mathbf{J}_t)),\tag{8}$$

where $k\in\{1,2,\dots,n\}$. Noteworthily, if the LE calculation results in a complex number, only the real part of the result is considered [40]. By observing Eq. (8), we can learn that the values of the n LEs of nD-CS can be inferred from the singular values of $\mathbf{J}_t$. Therefore, we introduce Theorem 1 [41] and Theorem 2 [42] to explore the characteristics of the singular values of $\mathbf{J}_t$.

Theorem 1 ([41]). *Suppose the singular values of a matrix are arranged in non-increasing order, i.e., $\sigma_1\geq\sigma_2\geq\cdots\geq\sigma_n$. Then, for any two matrices $\mathbf{A},\mathbf{B}\in\mathbb{C}^{n\times n}$, they hold that $\sigma_k(\mathbf{AB})\geq\max\{\sigma_k(\mathbf{A})\sigma_n(\mathbf{B}),\sigma_k(\mathbf{B})\sigma_n(\mathbf{A})\}$ for $k\in\{1,2,\dots,n\}$.*

Theorem 2 ([42]). *For a matrix $\mathbf{A}=(a_{pq})\in\mathbb{C}^{n\times n}$, let us denote $r_k=\sum_{q=1,q\neq k}^{n}|a_{kq}|$ and $c_k=\sum_{p=1,p\neq k}^{n}|a_{pk}|$ for $k\in\{1,2,\dots,n\}$ as the sum of the absolute values of the off-diagonal elements in row k and column k of $\mathbf{A}$, respectively. Moreover, we denote $s_k=\max\{r_k,c_k\}$. Then, all the singular values of $\mathbf{A}$ are included in $\bigcup_{k=1}^{n}I_k$, where $I_k=[(|a_{kk}|-s_k)^+,|a_{kk}|+s_k]$ and $(\cdot)^+=\max\{0,\cdot\}$.*

According to Theorem 1 and Eq. (5), the minimum singular value of $\mathbf{J}_t$ can be expressed as

$$\begin{aligned}\sigma_n(\mathbf{J}_t)&=\sigma_n(\mathbf{J}_{\mathbf{x}_{t-1}}\mathbf{J}_{t-1})\\&\geq\sigma_n(\mathbf{J}_{\mathbf{x}_{t-1}})\sigma_n(\mathbf{J}_{t-1})\\&\geq\sigma_n(\mathbf{J}_{\mathbf{x}_{t-1}})\sigma_n(\mathbf{J}_{\mathbf{x}_{t-2}})\cdots\sigma_n(\mathbf{J}_{\mathbf{x}_0})\\&=\prod_{i=0}^{t-1}\sigma_n(\mathbf{J}_{\mathbf{x}_i}),\end{aligned}\tag{9}$$

where $\sigma_n(\mathbf{J}_{\mathbf{x}_i})$ is the minimum singular value of $\mathbf{J}_{\mathbf{x}_i}$ and $i\in\{0,1,\dots,t-1\}$. Furthermore, according to Theorem 2 and Eq. (6), all the singular values of $\mathbf{J}_{\mathbf{x}_i}$ are bounded within the following interval

$$\bigcup_{k=1}^{n}I_k=\bigcup_{k=1}^{n}[(|l_k|-s_k)^+,|l_k|+s_k],\tag{10}$$

where $s_k=\max\{r_k,c_k\}$, $r_k=\sum_{q=1,q\neq k}^{n}\left|f_{(q-k)\bmod n}(x_{q,i})\right|$, and $c_k=\sum_{p=1}^{n-1}\left|f_p(x_{k,i})\right|$. As observed, s_k (or r_k, c_k) is the sum of the absolute values of each function $f(\cdot)\in\mathbb{D}$ at some point $x\in[0,M)$, and the lower bound of the singular values of $\mathbf{J}_{\mathbf{x}_i}$ is determined by the expression $\left(|l_k|-s_k\right)^+$. Therefore, if $\left(|l_k|-s_k\right)^+>1$ holds for $k\in\{1,2,\dots,n\}$, all the singular values of $\mathbf{J}_{\mathbf{x}_i}$ are greater than 1, indicating $\sigma_n(\mathbf{J}_t)>1$ according to Eq. (9).

Based on the above analysis, we present Proposition 1 to state the condition for nD-CS to exhibit chaotic behavior and provide the proof.

Proposition 1. *The nD-CS can exhibit chaotic behavior if*

$$|l_k|>1+\sum_{j=1}^{n-1}\max\left(\left|f_j(x)\right|_{x\in[0,M)}\right)\tag{11}$$

holds for $k\in\{1,2,\dots,n\}$.

Proof. If Eq. (11) holds for $k\in\{1,2,\dots,n\}$, we can derive that

$$\begin{aligned}|l_k|-s_k&>1+\sum_{j=1}^{n-1}\max\left(\left|f_j(x)\right|_{x\in[0,M)}\right)-s_k\\&=1+\sum_{j=1}^{n-1}\max\left(\left|f_j(x)\right|_{x\in[0,M)}\right)-\sum_{j=1}^{n-1}\left|f_j(x)\right|_{x\in[0,M)}\\&\geq 1\end{aligned}\tag{12}$$

and

$$\left(|l_k|-s_k\right)^+=\max\left\{0,|l_k|-s_k\right\}=|l_k|-s_k>1.\tag{13}$$

Therefore, according to Eq. (10), the singular values of $\mathbf{J}_{\mathbf{x}_i}$ are all greater than 1, namely $\sigma_1(\mathbf{J}_{\mathbf{x}_i})\geq\sigma_2(\mathbf{J}_{\mathbf{x}_i})\geq\cdots\geq\sigma_n(\mathbf{J}_{\mathbf{x}_i})>1$. Furthermore, by combining Eq. (9), we can conclude that the minimum singular value of $\mathbf{J}_t$ satisfies that

$$\sigma_n(\mathbf{J}_t)\geq\prod_{i=0}^{t-1}\sigma_n(\mathbf{J}_{\mathbf{x}_i})>1.\tag{14}$$

Eventually, referring to the LE calculation method described in Eq. (8), we can calculate the LEs of nD-CS by

$$\mathrm{LE}_k \geq \lim_{t\to\infty} \frac{1}{t} \ln(\sigma_n(\mathbf{J}_t)) > 0, \tag{15}$$

where $k \in \{1, 2, \ldots, n\}$. Since the n LEs of nD-CS are all positive, and the outputs of nD-CS are globally bounded within $[0, M)^n$, conditions (1) and (2) of Definition 1 are satisfied. This implies that nD-CS exhibits chaotic behavior. Additionally, when the dimensionality of nD-CS is greater than 1, it can exhibit hyperchaotic behavior. This completes the proof of Proposition 1. □

The chaotic maps generated by nD-CS can show chaotic behaviors by ensuring that their control parameters surpass the boundary determined by Eq. (11). If a 1D chaotic map has the maximum absolute value of its derivative within $x \in [0, M)$, enabling it to satisfy Eq. (11), it can be utilized as the seed map. Hence, users have great flexibility to select the seed maps and control parameter values of nD-CS to generate their desired chaotic maps with robust and complex dynamic behavior.

3. Three 3D examples of nD-CS

This section presents three examples of new 3D chaotic maps generated by nD-CS and evaluates their performance.

3.1. Examples of new chaotic maps

We utilized nD-CS to generate three new 3D chaotic maps by employing the fraction [34], logistic [17], and sine [36] maps listed in Table 1 as seed maps. The control parameters of these seed maps were set to their typical values: 1 for the fraction map, 4 for the logistic map, and 1 for the sine map. The modulus coefficient of nD-CS was set to $M = 1$ for simplicity. Thus, when $x \in [0, 1)$ and the control parameter of each seed map is set to its typical value, the maximum absolute values of the derivatives (i.e., $\max(|f|)$) for the fraction, logistic, and sine maps are calculated as 21.5396, 4, and π, respectively.

3.1.1. 3D Fraction-Logistic Circularly Shifting chaotic map

When using the fraction and logistic maps as the seed maps of nD-CS, the 3D Fraction-Logistic Circularly Shifting (3D-FL-CS) chaotic map can be generated. The mathematical representation of the 3D-FL-CS is defined as

$$\begin{cases} x_{1,i+1} = l_1 x_{1,i} + \frac{1}{x_{2,i}^2+0.1} - x_{2,i} + 4x_{3,i}(1-x_{3,i}) \mod 1 \\ x_{2,i+1} = 4x_{1,i}(1-x_{1,i}) + l_2 x_{2,i} + \frac{1}{x_{3,i}^2+0.1} - x_{3,i} \mod 1 \\ x_{3,i+1} = \frac{1}{x_{1,i}^2+0.1} - x_{1,i} + 4x_{2,i}(1-x_{2,i}) + l_3 x_{3,i} \mod 1, \end{cases} \tag{16}$$

where l_1, l_2, and l_3 are the control parameters of the 3D-FL-CS. According to Proposition 1, the control parameters l_k ($k \in \{1, 2, 3\}$) should satisfy the following equation in order for the 3D-FL-CS to exhibit chaotic behavior:

$$|l_k| > 1 + \sum_{j=1}^{2} \max\left(|f_j(x)|_{x\in[0,1)}\right) > 1 + 21.5396 + 4 = 26.5396. \tag{17}$$

3.1.2. 3D Fraction-Sine Circularly Shifting chaotic map

By utilizing the fraction and sine maps as the seed maps of nD-CS, we can construct the 3D Fraction-Sine Circularly Shifting (3D-FS-CS) chaotic map. The mathematical definition of the 3D-FS-CS is shown as

$$\begin{cases} x_{1,i+1} = l_1 x_{1,i} + \frac{1}{x_{2,i}^2+0.1} - x_{2,i} + \sin(\pi x_{3,i}) \mod 1 \\ x_{2,i+1} = \sin(\pi x_{1,i}) + l_2 x_{2,i} + \frac{1}{x_{3,i}^2+0.1} - x_{3,i} \mod 1 \\ x_{3,i+1} = \frac{1}{x_{1,i}^2+0.1} - x_{1,i} + \sin(\pi x_{2,i}) + l_3 x_{3,i} \mod 1, \end{cases} \tag{18}$$

where l_1, l_2, and l_3 are the control parameters. It has been demonstrated in Proposition 1 that the 3D-FS-CS can exhibit chaotic behavior when its control parameters l_k ($k \in \{1, 2, 3\}$) satisfy that

$$|l_k| > 1 + \sum_{j=1}^{2} \max\left(|f_j(x)|_{x\in[0,1)}\right) > 1 + 21.5396 + \pi = 25.6812. \tag{19}$$

3.1.3. 3D Logistic-Sine Circularly Shifting chaotic map

The 3D Logistic-Sine Circularly Shifting (3D-LS-CS) chaotic map is generated by utilizing the logistic and sine maps as the seed maps of nD-CS. Therefore, the mathematical expression of the 3D-LS-CS is defined as

$$\begin{cases} x_{1,i+1} = l_1 x_{1,i} + 4x_{2,i}(1-x_{2,i}) + \sin(\pi x_{3,i}) \mod 1 \\ x_{2,i+1} = \sin(\pi x_{1,i}) + l_2 x_{2,i} + 4x_{3,i}(1-x_{3,i}) \mod 1 \\ x_{3,i+1} = 4x_{1,i}(1-x_{1,i}) + \sin(\pi x_{2,i}) + l_3 x_{3,i} \mod 1, \end{cases} \tag{20}$$

where l_1, l_2, and l_3 are the control parameters. According to Proposition 1, the 3D-LS-CS can show chaotic behavior when its control parameters l_k ($k \in \{1, 2, 3\}$) satisfy that

$$|l_k| > 1 + \sum_{j=1}^{2} \max\left(|f_j(x)|_{x\in[0,1)}\right) > 1 + 4 + \pi = 8.1416. \tag{21}$$

3.2. Performance evaluation

The performance of the newly generated 3D-FL-CS, 3D-FS-CS, and 3D-LS-CS is experimentally evaluated from several aspects: LE, sample entropy (SE), correlation dimension (CD), information entropy (IE), randomness test, trajectory, and fixed-point stability. The control parameters and initial states of the three 3D chaotic maps for different evaluation indicators are listed in Table 2. The LEs of each chaotic map are studied within a specified control parameter range, while the control parameters of each chaotic map are randomly selected for the remaining evaluation indicators. The initial states of each chaotic map are randomly selected within $[0, 1)^3$.

3.2.1. LE

As mentioned in Definition 1, a globally bounded dynamic system exhibits chaotic behavior if it has at least one positive LE, and hyperchaotic behavior if it has more than one positive LE. Fig. 1 depicts the three LEs of each newly generated 3D chaotic map, with different colors representing different LE values. It can be observed that all three LEs of the chaotic maps are positive across the entire parameter space, indicating their capability to exhibit hyperchaotic behavior. This observation further emphasizes the effectiveness of the nD-CS framework in generating chaotic maps with robust and complex dynamics. Moreover, larger control parameter values correspond to larger LEs. Thus, by adjusting the control parameter values in the nD-CS framework, the generated chaotic maps can achieve larger positive LEs and exhibit more complex dynamic behavior.

3.2.2. SE

The SE is a type of entropy used to measure the irregularity of a sequence produced by a chaotic map [43]. A positive SE means that the produced sequence shows irregular behavior, implying that the output of the chaotic map is hard to predict. A larger SE value indicates a higher level of irregularity. We apply the SE computation method provided in [43] to determine the SE of the chaotic sequence. The formula for SE is expressed as [43]:

$$\mathrm{SE} = -\ln\left(A^m(r)/B^m(r)\right), \tag{22}$$

where m represents the length of the compared segment, and r indicates the tolerance for accepting matches. For a sequence with N points $\{u_j\}_{j=1}^{N}$, it forms $N - m + 1$ vectors $\mathbf{x}_i^m = \{u_{i+k}\}_{k=0}^{m-1}$ for $i \in \{1, 2, \ldots, N - m + 1\}$. The distance between two such vectors is denoted as $d(\mathbf{x}_i^m, \mathbf{x}_j^m) = \max\left(\left|u_{i+k} - u_{j+k}\right|_{k\in\{0,1,\ldots,m-1\}}\right)$. Then, the number of vectors $\mathbf{x}_j^m$ within

Table 2
The control parameters and initial states of the 3D-FL-CS, 3D-FS-CS, and 3D-LS-CS for different evaluation indicators.

	Chaotic map	Different evaluation indicators	
		LE	SE, CD, IE, Randomness test, and Trajectory
Control parameters	3D-FL-CS	$l_1, l_2, l_3 \in [27, 126]$	$(l_1, l_2, l_3) = (122, 75, 107)$
	3D-FS-CS	$l_1, l_2, l_3 \in [26, 125]$	$(l_1, l_2, l_3) = (31, 49, 61)$
	3D-LS-CS	$l_1, l_2, l_3 \in [9, 108]$	$(l_1, l_2, l_3) = (38, 83, 27)$
Initial states	3D-FL-CS	$\mathbf{x}_0 = (x_{1,0}, x_{2,0}, x_{3,0}) = (0.1419, 0.4218, 0.9157)$	
	3D-FS-CS	$\mathbf{x}_0 = (x_{1,0}, x_{2,0}, x_{3,0}) = (0.8212, 0.0154, 0.0430)$	
	3D-LS-CS	$\mathbf{x}_0 = (x_{1,0}, x_{2,0}, x_{3,0}) = (0.6868, 0.1835, 0.3685)$	

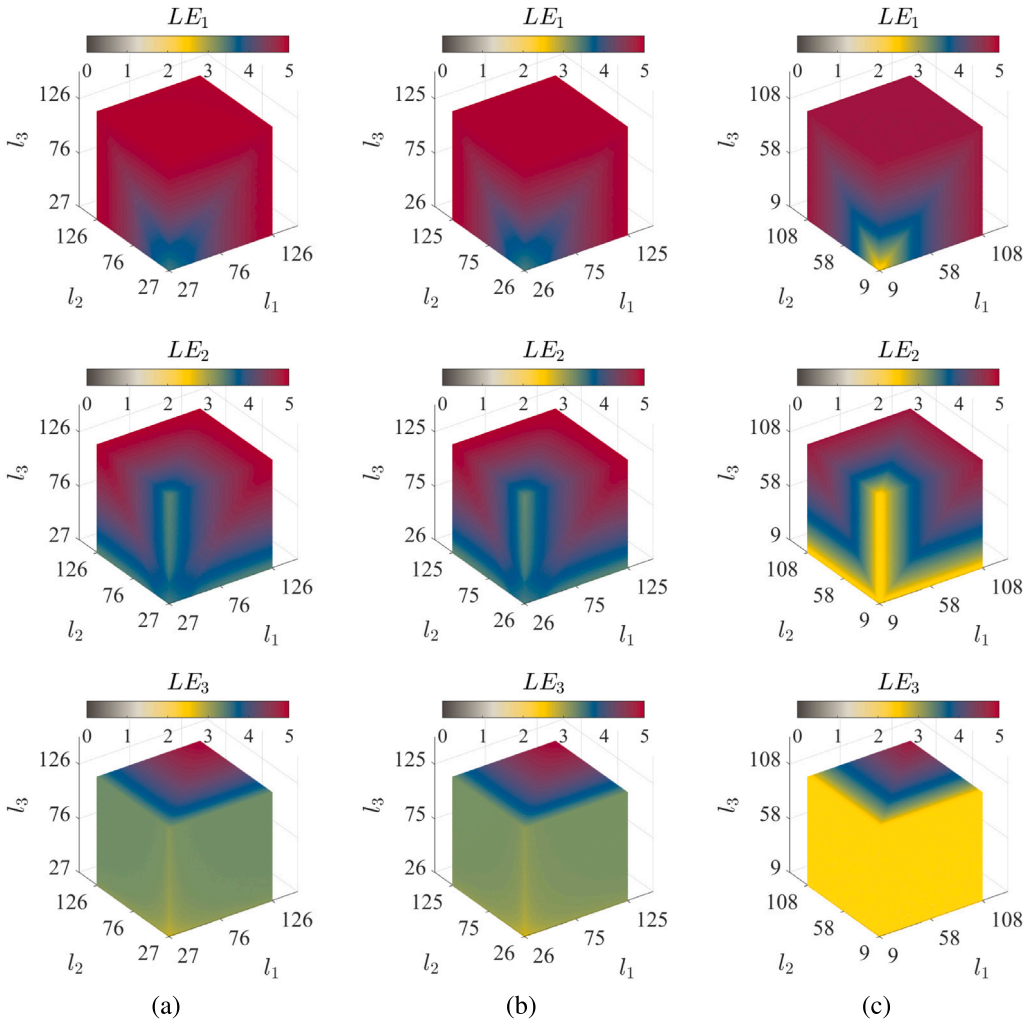

Fig. 1. The three LEs of (a) the 3D-FL-CS chaotic map, (b) the 3D-FS-CS chaotic map, and (c) the 3D-LS-CS chaotic map. (For interpretation of the references to color in this figure legend, the reader is referred to the web version of this article.)

r of $\mathbf{x}_i^m$ is expressed as $B_i^m(r)$, while the number of vectors $\mathbf{x}_j^{m+1}$ within r of $\mathbf{x}_i^{m+1}$ is defined as $A_i^m(r)$. Therefore, $B^m(r) = (N-m)^{-1}\sum_{i=1}^{N-m}(N-m-1)^{-1}B_i^m(r)$ refers to the probability that two sequences will match for m points, and $A^m(r) = (N-m)^{-1}\sum_{i=1}^{N-m}(N-m-1)^{-1}A_i^m(r)$ represents the probability that two sequences will match for $m+1$ points. In our experiment, we set $m = 2$ and $r = 0.2$std in accordance with [43], where std refers to the standard deviation of the sequence, to explore the SE of a chaotic sequence with a length of $N = 10{,}000$.

In the case of a high-dimensional chaotic map, each dimension's output forms an individual sequence. Therefore, three SE values can be calculated for a 3D chaotic map. Table 3 presents the obtained SE values and their average, denoted as $\overline{\text{SE}}$. It is evident that the SE values of the three newly generated 3D chaotic maps are all positive, indicating the presence of irregular outputs from these chaotic maps. Furthermore, the standard deviation of the three SEs for each chaotic map, denoted as std(SE), is relatively small, suggesting high consistency in irregularities across all dimensions for each chaotic map. Around the three chaotic maps, the 3D-FL-CS exhibits better SE performance than the other two. Moreover, the standard deviation of the $\overline{\text{SE}}$s of the three 3D chaotic maps, denoted as std($\overline{\text{SE}}$), is approximately 10^{-3}, illustrating the stable performance of the nD-CS-generated chaotic maps in terms of SE.

3.2.3. CD

The CD is a type of fractal dimension that quantifies the spatial dimensionality occupied by the sequence produced by a chaotic map [44]. It serves as a useful tool for assessing the existence and complexity of a strange attractor in a dynamic system. A positive CD

Table 3
The SE values and average SE for each of our 3D chaotic maps.

	SE_1	SE_2	SE_3	std(SE)	$\overline{SE}$
3D-FL-CS	2.1860	**2.1950**	2.1886	**0.0047**	**2.1899**
3D-FS-CS	**2.1936**	2.1874	2.1827	0.0055	2.1879
3D-LS-CS	2.1890	2.1825	**2.1923**	0.0050	2.1879
std($\overline{SE}$)					0.0011

Table 4
The CD values and average CD for each of our 3D chaotic maps.

	CD_1	CD_2	CD_3	std(CD)	$\overline{CD}$
3D-FL-CS	**1.9688**	1.9660	**1.9685**	**0.0015**	1.9678
3D-FS-CS	1.9633	1.9672	1.9614	0.0030	1.9640
3D-LS-CS	1.9642	**1.9764**	1.9665	0.0065	**1.9690**
std($\overline{CD}$)					0.0026

value indicates the presence of a strange attractor in the dynamic system, and a larger CD value suggests that the generated sequence occupies a higher spatial dimensionality, indicating more complex dynamic behavior of the system. We employ the CD calculation method introduced in [44] to compute the CD for the sequence generated by the chaotic map. For a sequence with N points $\{v_i\}_{i=1}^{N}$, where m is the embedding dimension and r represents the similarity scalar, the CD value is calculated as [44]

$$\mathrm{CD} = \lim_{r\to 0}\lim_{N\to \mathrm{inf}} \frac{\log(C_m(r))}{\log(r)}. \tag{23}$$

The investigated sequence constructs a vector-valued series $\{\mathbf{v}_i\}_{i=1}^{N-m+1}$ where $\mathbf{v}_i = [v_i, v_{i+1}, \ldots, v_{i+m-1}]^T$, leading the correlation sum function defined as [44]

$$C_m(r) = \frac{2\sum_{i<j}\theta(\|\mathbf{v}_i - \mathbf{v}_j\| - r)}{(N-m)(N-m+1)}, \tag{24}$$

where $\theta(\cdot)$ is the Heaviside step function, and $\|\cdot\|$ is usually a p-norm, defined as $\|\mathbf{x}\| = [\sum_i |x_i|^p]^{1/p}$. In our experiment, we set the embedding dimension m as 2 to explore the CD of a chaotic sequence with a length of $N = 10{,}000$.

Similar to SE, a 3D chaotic map can calculate three CD values, and the results are presented in Table 4. It can be seen that the CD values of the chaotic maps are all positive, revealing that the chaotic sequences produced by our chaotic maps occupy a high spatial dimensionality. Additionally, among the three chaotic maps, the 3D-LS-CS exhibits a larger average CD value than the other two. Furthermore, the relatively small standard deviations of the CDs affirm the stability of the performance of the chaotic maps generated by our nD-CS.

3.2.4. IE

The IE is a quantitative measure of the uncertainty or randomness within a given set of data [45]. It can be used to evaluate the uncertainty of the chaotic sequences generated by a chaotic map. For an nD chaotic map, it produces n chaotic sequences, and its phase space can be divided into multiple subspaces. Specifically, if the output of each dimension of an nD chaotic map is uniformly divided into P parts, then the entire phase space can be divided into P^n subspaces. Hence, the IE of the chaotic sequences generated by an nD chaotic map can be calculated as

$$\mathrm{IE} = -\sum_{t=1}^{P^n} \Pr(t)\log_2(\Pr(t)), \tag{25}$$

where $\Pr(t)$ represents the probability that the output state falls into the tth subspace. It can be observed from the equation above that the IE value can reach a theoretical maximum value $\mathrm{IE}_{max} = n\log_2(P)$ when the probability of a state falling into each subspace is the same, i.e., $\Pr(t) = 1/P^n$ holds for $t \in \{1, 2, \ldots, P^n\}$. A larger IE value indicates a higher degree of randomness for the generated states, and a larger P value allows for more precise measurements of the IE value.

Table 5 presents the IE values of our 3D-FL-CS, 3D-FS-CS, and 3D-LS-CS chaotic maps for various P values. The states generated by each chaotic map have a length of P^4. It is evident from the results that the IE values of our maps consistently approach the theoretical maximum IE value. This indicates that the sequences generated by our maps exhibit a high degree of uncertainty. Among the three chaotic maps, both the 3D-FS-CS and the 3D-LS-CS exhibit better IE performance than the 3D-FL-CS.

3.2.5. Randomness test

Due to the limited precision of digital platforms, a chaotic map implemented on such platforms may eventually degrade to periodic behavior as the evolution time increases. This phenomenon is known as chaos degradation. However, a chaotic map with more robust chaotic behavior demonstrates stronger ability to delay chaos degradation, which is more desirable for practical applications. In this context, we assess the ability of our newly generated chaotic maps by testing the randomness of the sequences they produce. A chaotic map exhibits a stronger ability to delay chaos degradation if it can generate longer chaotic sequences that pass the randomness test.

Among the various randomness test standards, the TestU01 standard [46] is known for its stringent assessment of large amounts of data from multiple perspectives. The TestU01 standard consists of eight test batteries: SmallCrush, Crush, BigCrush, Alphabit, BlockAlphabit, Rabbit, PseudoDieHARD and FIPS-140-2. The PseudoDIEHARD battery encompassses most of the tests from the DIEHARD standard [47], while the FIPS-140-2 battery includes a small suite of tests from the NIST standard [48]. Each test battery comprises several subtests, with each subtest generating a p-value when a chaotic sequence is evaluated. The tested data is considered to pass the subtest if the resulting p-value falls within the range of $[0.001, 0.999]$. Additionally, the BigCrush, Crush, SmallCrush, PseudoDIEHARD, and FIPS-140-2 batteries utilize default test data sizes, while the remaining batteries allow for user-specified test data sizes. The BigCrush battery is typically designated for high-volume testing and operates with a test data size of approximately 10Tb. In our experiment, we set the test data sizes for Rabbit, Alphabit, and BlockAlphabit batteries to 1 Gb. Moreover, the output of each dimension of every chaotic map serves as the test sequence for TestU01. Eight bits are extracted from each dimensional output to compose the sequence within its dimension. Table 6 presents the test results for the three new 3D chaotic maps. It is evident that our chaotic maps successfully pass all subtests across all test batteries, and the three chaotic maps perform equally well. This result suggests that the sequences generated by our chaotic maps exhibit a high level of randomness, indicating a strong capability to delay chaos degradation.

3.2.6. Trajectory

For a chaotic map, the trajectory represents a collection of points visited in phase space, providing insight into its behavior as it evolves from an initial state. This visualization aids in understanding the distribution of the chaotic map's outputs. We present the trajectories of the three newly generated 3D chaotic maps in Fig. 2, with their parameter settings and initial states listed in Table 2. As illustrated in Fig. 2, the initial state of each chaotic map is indicated by a red star, and the trajectories of our chaotic maps are uniformly distributed, covering the entire phase space without any discernible structure. This illustrates the high level of randomness exhibited by the chaotic maps' outputs.

3.2.7. Fixed-point stability

A fixed point is a point that is mapped to itself by a function. Depending on its stability, a fixed point can be classified as either stable or unstable. A stable fixed point means that other states near the fixed point are attracted to it, and the dynamic system remains stabilized as iterations progress, corresponding to the periodic behavior of the

Table 5
The IE values of the 3D-FL-CS, 3D-FS-CS, and 3D-LS-CS chaotic maps against different P values.

P	3	5	7	9	11	13	15	17	19	21	23
IE_{max}	4.7549	6.9658	8.4221	9.5098	10.3783	11.1013	11.7207	12.2624	12.7438	13.1770	13.5707
3D-FL-CS	4.4458	6.7956	8.3180	9.4276	10.3098	11.0461	11.6714	12.2190	12.7048	13.1422	13.5390
3D-FS-CS	4.5056	**6.8595**	**8.3357**	9.4226	**10.3125**	11.0463	**11.6721**	12.2200	12.7048	13.1418	**13.5395**
3D-LS-CS	**4.5428**	6.8061	8.3103	**9.4323**	10.3106	**11.0473**	11.6708	**12.2215**	**12.7059**	**13.1432**	13.5393

Table 6
The TestU01 test results of the 3D-FL-CS, 3D-FS-CS, and 3D-LS-CS chaotic maps.

Test batteries	Data size	3D-FL-CS			3D-FS-CS			3D-LS-CS		
		1st	2nd	3rd	1st	2nd	3rd	1st	2nd	3rd
SmallCrush	≈ 6 Gb	15/15	15/15	15/15	15/15	15/15	15/15	15/15	15/15	15/15
Crush	≈ 1 Tb	144/144	144/144	144/144	144/144	144/144	144/144	144/144	144/144	144/144
BigCrush	≈ 10 Tb	160/160	160/160	160/160	160/160	160/160	160/160	160/160	160/160	160/160
Alphabit	1 Gb	17/17	17/17	17/17	17/17	17/17	17/17	17/17	17/17	17/17
BlockAlphabit	1 Gb	102/102	102/102	102/102	102/102	102/102	102/102	102/102	102/102	102/102
Rabbit	1 Gb	40/40	40/40	40/40	40/40	40/40	40/40	40/40	40/40	40/40
PseudoDIEHARD	≈ 5 Gb	126/126	126/126	126/126	126/126	126/126	126/126	126/126	126/126	126/126
FIPS-140–2	≈ 19 Kb	16/16	16/16	16/16	16/16	16/16	16/16	16/16	16/16	16/16

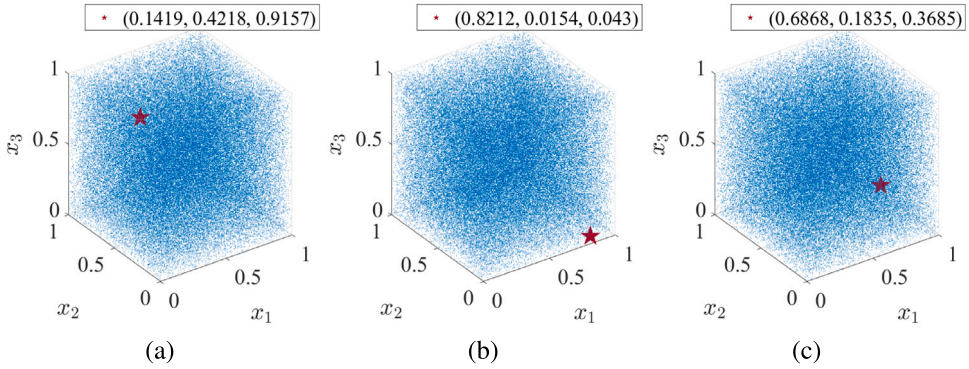

Fig. 2. The trajectories of (a) the 3D-FL-CS chaotic map, (b) the 3D-FS-CS chaotic map, and (c) the 3D-LS-CS chaotic map.

dynamic system. On the contrary, an unstable fixed point indicates that other states near the fixed point are repelled by it, and the dynamic system keeps oscillating, corresponding to the chaotic behavior of the dynamic system.

The stability of a fixed point can be determined by examining the gradient of the dynamic system at that point. For a 3D dynamic system, the gradient at a specific point is determined by the three eigenvalues (λ_1, λ_2, and λ_3) of the Jacobian matrix (as presented in Eq. (6)) of the system at that point. A fixed point is considered unstable if $|\lambda_j| > 1$ holds for $j \in \{1, 2, 3\}$; otherwise, it is considered stable. The fixed points of our three newly generated 3D chaotic maps, denoted as $(\tilde{x}_1, \tilde{x}_2, \tilde{x}_3)$, are the solutions of the following equations:

$$\begin{cases} \tilde{x}_1 = l_1\tilde{x}_1 + \frac{1}{\tilde{x}_2^2+0.1} - \tilde{x}_2 + 4\tilde{x}_3(1-\tilde{x}_3) \mod 1 \\ \tilde{x}_2 = 4\tilde{x}_1(1-\tilde{x}_1) + l_2\tilde{x}_2 + \frac{1}{\tilde{x}_3^2+0.1} - \tilde{x}_3 \mod 1 \\ \tilde{x}_3 = \frac{1}{\tilde{x}_1^2+0.1} - \tilde{x}_1 + 4\tilde{x}_2(1-\tilde{x}_2) + l_3\tilde{x}_3 \mod 1, \end{cases} \tag{26a}$$

$$\begin{cases} \tilde{x}_1 = l_1\tilde{x}_1 + \frac{1}{\tilde{x}_2^2+0.1} - \tilde{x}_2 + \sin(\pi\tilde{x}_3) \mod 1 \\ \tilde{x}_2 = \sin(\pi\tilde{x}_1) + l_2\tilde{x}_2 + \frac{1}{\tilde{x}_3^2+0.1} - \tilde{x}_3 \mod 1 \\ \tilde{x}_3 = \frac{1}{\tilde{x}_1^2+0.1} - \tilde{x}_1 + \sin(\pi\tilde{x}_2) + l_3\tilde{x}_3 \mod 1, \end{cases} \tag{26b}$$

$$\begin{cases} \tilde{x}_1 = l_1\tilde{x}_1 + 4\tilde{x}_2(1-\tilde{x}_2) + \sin(\pi\tilde{x}_3) \mod 1 \\ \tilde{x}_2 = \sin(\pi\tilde{x}_1) + l_2\tilde{x}_2 + 4\tilde{x}_3(1-\tilde{x}_3) \mod 1 \\ \tilde{x}_3 = 4\tilde{x}_1(1-\tilde{x}_1) + \sin(\pi\tilde{x}_2) + l_3\tilde{x}_3 \mod 1. \end{cases} \tag{26c}$$

Table 7 displays the fixed points of the three 3D chaotic maps under various control parameter settings, along with the absolute eigenvalues of their Jacobian matrices at these fixed points. We have included only the fixed points corresponding to several representative parameter settings, using dots to represent omitted experimental results. As observed, each chaotic map exhibits multiple fixed points under different parameter settings. Moreover, the absolute eigenvalues of the Jacobian matrix at each fixed point are all greater than 1, indicating the instability of all the fixed points. This further confirms the chaotic behavior demonstrated by our chaotic maps.

4. Performance comparison

This section compares the chaotic maps generated by our nD-CS with existing chaotic map generation methods using LE, SE, CD, and IE indicators. To generate our chaotic maps, we randomly select 1D chaotic maps from Table 1 as seed maps. The map IDs of selected seed maps for different investigated dimensions are listed in Table 8. To ensure chaotic behavior, the control parameters of our chaotic maps must meet specific conditions according to Proposition 1. As a result, the control parameters for each of our chaotic maps are randomly chosen from the range associated with the given condition listed in Table 8. The lower bound of the range is the smallest integer greater than the condition, and the upper bound is 500 more than the lower bound for a comprehensive investigation. For example, when generating our 3D chaotic maps, we randomly select their control parameters within the range [25, 525]. Moreover, the initial state of each of our chaotic maps is set as $\mathbf{x}_0 = \{0.5\}^{n\times 1}$.

For the nD chaotic maps generated by previous methods proposed by Natiq et al. [30], Zang et al. [28], Huang et al. [31], and Zhang et al. [29], their control parameters are chosen at random from

Table 7
The fixed points of the 3D-FL-CS, 3D-FS-CS, and 3D-LS-CS chaotic maps, the absolute eigenvalues of their Jacobian matrices at the respective fixed points, and the stability of the fixed points.

Chaotic map	Control parameters (l_1, l_2, l_3)	Fixed points $(\tilde{x}_1, \tilde{x}_2, \tilde{x}_3)$	Absolute eigenvalues $(\lvert\lambda_1\rvert, \lvert\lambda_2\rvert, \lvert\lambda_3\rvert)$	Stability
3D-FL-CS	(27, 28, 29)	(0, 0, 0)	(26.8011, 26.8011, 31.0775)	unstable
		(0.2025, 0.0682, 0.0663)	(37.8848, 37.8848, 15.6067)	unstable
		(0.5914, 0.0224, 0.2243)	(21.4650, 33.1587, 33.1587)	unstable
	(30, 31, −32)	(0, 0, 0)	(30.4729, 30.4729, 31.8556)	unstable
		(0.4141, 0.3059, 0.0339)	(31.4898, 30.8576, 30.8576)	unstable
		(0.5139, 0.2205, 0.1794)	(31.8871, 31.4290, 31.4290)	unstable
		(0.6639, 0.3034, 0.6979)	(32.1398, 26.6700, 34.4698)	unstable
	...	...	...	...
3D-FS-CS	(26, 27, 28)	(0, 0, 0)	(26.1163, 26.1163, 29.2355)	unstable
		(0.7987, 0.1490, 0.4812)	(16.4951, 33.1204, 33.1204)	unstable
		(0.9079, 0.4835, 0.2899)	(17.8115, 32.2543, 32.2543)	unstable
	(29, 30, −31)	(0, 0, 0)	(29.4846, 29.4846, 30.8878)	unstable
		(0.9636, 0.4315, 0.4058)	(30.9303, 24.0394, 34.8910)	unstable
	...	...	...	...
3D-LS-CS	(9, 10, 11)	(0, 0, 0)	(17.2034, 6.4153, 6.4153)	unstable
		(0, 0, 0.5000)	(5.9200, 13.0800, 11.0000)	unstable
		(0.5000, 0, 0)	(9.0000, 6.9200, 14.0800)	unstable
		(0.5000, 0, 0.5000)	(9, 11, 10)	unstable
	(12, 13, −14)	(0, 0, 0)	(16.9134, 8.8935, 14.8068)	unstable
		(0, 0.5000, 0)	(14.4747, 12.4747, 13.0000)	unstable
	...	...	...	...

Table 8
Configurations of our nD-CS for generating nD chaotic maps with respect to different dimensions from 3 to 12.

Dimension n	Map IDs of the seed maps from F_1 to F_{n-1}	Condition of the control parameters for $k \in \{1, 2, \ldots, n\}$	Used parameter range
3	5,3	$\lvert l_k\rvert > 24.5396$	[25,525]
4	6, 5, 3	$\lvert l_k\rvert > 27.6812$	[28,528]
5	3, 5, 6, 3	$\lvert l_k\rvert > 49.2208$	[50,550]
6	6, 3, 4, 3, 5	$\lvert l_k\rvert > 53.2208$	[54,554]
7	5, 4, 6, 3, 2, 3	$\lvert l_k\rvert > 56.2208$	[57,557]
8	1, 4, 2, 3, 5, 6, 3	$\lvert l_k\rvert > 60.2208$	[61,561]
9	4, 3, 3, 6, 5, 3, 1, 2	$\lvert l_k\rvert > 81.7604$	[82,582]
10	3, 3, 2, 3, 4, 1, 5, 4, 6	$\lvert l_k\rvert > 85.7604$	[86,586]
11	6, 1, 3, 3, 3, 2, 2, 4, 4, 5	$\lvert l_k\rvert > 88.7604$	[89,589]
12	2, 3, 4, 2, 1, 3, 4, 5, 6, 5, 3	$\lvert l_k\rvert > 90.7604$	[91,591]

Table 9
Configurations of the competing chaotic map generation methods, where the settings of their control parameters follow their original papers.

Competing chaotic map generation methods	Control parameters	Initial state
Natiq et al.'s [30]	$\beta = 6,\ \sigma \in [\pi, 3\pi],\ \mu \in [1, 8]$	$\mathbf{x}_0 = \{0.5\}^{n\times 1}$
Zang et al.'s [28]	$t = \lceil 1 + \max_{k\in\{1..n\}}\left(\sum_{j=1,j\neq k}^{n} \lvert a_{k,j}\rvert\right)\rceil,\ a_{i,i} = t$ for $i \in \{1, 2, \ldots, n\}$, $a_{i,j} \in [-1, 1]$ for $i \neq j$	
Huang et al.'s [31]	$\mu = 1,\ k \in [1, 10]$	
Zhang et al.'s [29]	$b_i \in [1, 6]$ for $i \in \{1, 2, \ldots, n\}$	

the ranges specified in their original papers, and their initial states are also set to $\mathbf{x}_0 = \{0.5\}^{n\times 1}$, as listed in Table 9. To elaborate, Zang et al.'s nD chaotic maps are generated based on the strictly over-one diagonally dominant matrix introduced in its original paper. Huang et al.'s nD chaotic maps are generated using the linear function as the seed function. Zhang et al.'s nD chaotic maps are generated using their cyclic symmetric Chebyshev framework. For each method of generating chaotic maps, we generate 100 maps for every dimension and calculate their average indicators for the following comparisons.

4.1. LE comparison

This part compares the chaotic maps generated by our nD-CS with those of the competing nD chaotic map generation methods from the perspective of LE. Since an nD chaotic map can calculate n LEs, we take the largest LE (LLE) of each nD chaotic map as the representative LE to reveal its dynamic behavior. Then, the average LLE of the 100 chaotic maps generated by each nD chaotic map generation method for each investigated dimension n is computed, and the obtained results are listed in Fig. 3. As shown, the chaotic maps generated by our nD-CS have significantly larger LLEs in every investigated dimension than those generated by the competing methods, suggesting that our chaotic maps can exhibit more complex dynamic behavior than previous methods.

Furthermore, we also compare the number of positive LEs of the generated chaotic maps, and Table 10 lists the average number of positive LEs of the 100 chaotic maps generated by each nD chaotic map generation method for each investigated dimension. It can be seen that our nD-CS, Zang et al.'s method, and Zhang et al.'s method consistently generate nD chaotic maps with n positive LEs, whereas other methods cannot. This demonstrates that our nD-CS can always generate chaotic maps exhibiting robust hyperchaotic behavior and n positive LEs.

Table 10
The average number of positive LEs of chaotic maps generated by different nD chaotic map generation methods with dimension $n \in \{3, 4, \ldots, 12\}$.

Dimension n	Ours	Natiq et al.'s [30]	Zang et al.'s [28]	Huang et al.'s [31]	Zhang et al.'s [29]
3	3	*1.97*	3	3	3
4	4	4	4	4	4
5	5	5	5	5	5
6	6	6	6	6	6
7	7	7	7	7	7
8	8	8	8	*7.99*	8
9	9	9	9	9	9
10	10	10	10	*9.97*	10
11	11	11	11	*10.99*	11
12	12	12	12	*11.99*	12

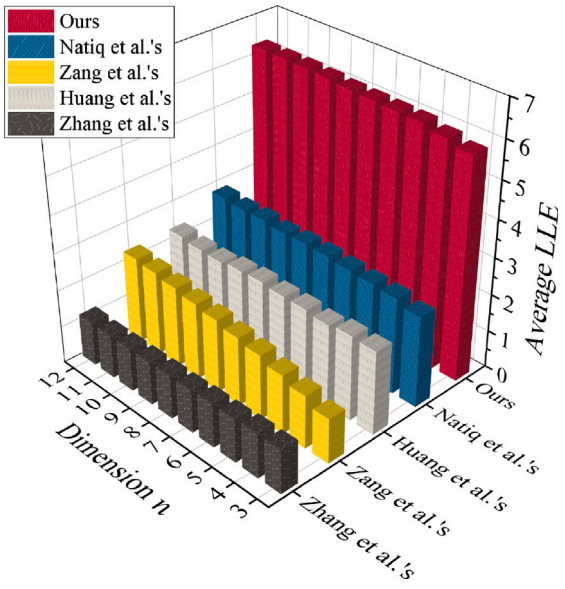

Fig. 3. The average LLE of chaotic maps generated by various nD chaotic map generation methods for investigated dimension $n \in \{3, 4, \ldots, 12\}$.

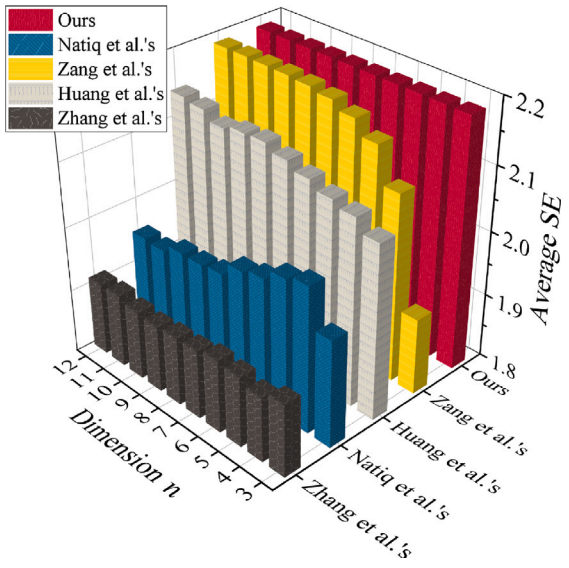

Fig. 4. The average SE of chaotic maps generated by each nD chaotic map generation method for investigated dimension $n \in \{3, 4, \ldots, 12\}$.

4.2. SE comparison

In this subsection, we compare our nD-CS with other nD chaotic map generation methods based on the SE. Since an nD chaotic map has n SEs, each corresponding to a sequence produced by a specific dimension of the chaotic map, we calculate the average value of the n SEs as the SE indicator of an nD chaotic map. Subsequently, we compute the SEs of the 100 chaotic maps generated by each method for each investigated dimension, and their average value serves as the final result, depicted in Fig. 4. As can be seen, the SEs of our chaotic maps consistently rank as the largest and maintain stability across different dimensions. In contrast, the SEs of competing nD chaotic maps are relatively small and exhibit unstable changes as the dimension n increases. For example, the SE of Natiq et al.'s nD chaotic maps boosts from $n = 3$ to $n = 4$ but subsequently declines, while the SEs of Zhang et al.'s and Huang et al.'s nD chaotic maps show dips at dimensions $n = 4$ and $n = 10$, respectively. Moreover, the SEs of Zang et al.'s nD chaotic maps are larger than Huang et al.'s except when $n = 3$. In summary, the results suggest that our nD-CS consistently ensures larger and stable SEs for the generated chaotic maps. This implies that chaotic maps generated by the proposed nD-CS exhibit lower level of regularity and more unpredictable outputs.

4.3. CD comparison

In this comparison, we conduct a comparative analysis of our nD-CS against other nD chaotic map generation methods using the CD perspective. Similar to the SE comparison, we calculate the average CD of the n CDs of an nD chaotic map as its CD indicator. Then, we calculate the average CD indicator of the 100 chaotic maps generated by each method for each investigated dimension as the final result. As depicted in Fig. 5, the chaotic maps generated by nD-CS consistently exhibit the largest CD across all investigated dimensions. The CDs of Zang et al.'s and Huang et al.'s nD chaotic maps closely approach ours, whereas the CDs of Natiq et al.'s and Zhang et al.'s are notably smaller. These results suggest that chaotic maps generated by our nD-CS possess a larger CD, indicating higher spatial dimensionality compared to those generated by other methods.

4.4. IE comparison

This subsection compares the performance of our nD-CS with other nD chaotic map generation methods from the perspective of IE. Two groups of experiments are conducted to calculate the IE of the sequences produced by different chaotic maps. The first group of experiments evaluates IE against investigated dimension $n \in \{3, 4, \ldots, 12\}$ while maintaining the number of divided parts $P = 3$. For each chaotic map generation method and each investigated dimension n, 100 nD chaotic maps are randomly generated. The initial state for each chaotic map is set to $\mathbf{x}_0 = \{0.5\}^{n\times 1}$, and a total of P^{n+1} output states are produced to calculate its IE. The average IE of the 100 chaotic maps generated by each method for each investigated dimension is calculated as the final IE indicator. Fig. 6 displays the average IEs of the 100 nD chaotic maps generated by different methods. The results illustrate that the nD chaotic maps generated by our nD-CS achieve higher IEs

Table 11
The average IE of chaotic maps generated by each nD chaotic map generation method for investigated dimension $n = 3$, with the number of divided parts $P \in \{3, 5, \ldots, 23\}$.

P	3	5	7	9	11	13	15	17	19	21	23
IE_{max}	4.7549	6.9658	8.4221	9.5098	10.3783	11.1013	11.7207	12.2624	12.7438	13.1770	13.5707
Ours	4.5058	6.8175	8.3166	9.4279	10.3114	11.0450	11.6721	12.2194	12.7055	13.1423	13.5391
Natiq et al.'s [30]	4.2469	6.5049	7.9325	8.9506	9.7715	10.4711	11.0473	11.5577	12.0106	12.4173	12.7875
Zang et al.'s [28]	4.5007	6.8133	8.3157	9.4273	10.3110	11.0440	11.6710	12.2185	12.7044	13.1411	13.5378
Huang et al.'s [31]	4.0371	6.4435	7.8858	8.9587	9.8398	10.5796	11.2020	11.7573	12.2459	12.6722	13.0880
Zhang et al.'s [29]	4.4137	6.6313	8.0572	9.1188	9.9653	10.6655	11.2677	11.7893	12.2525	12.6682	13.0475

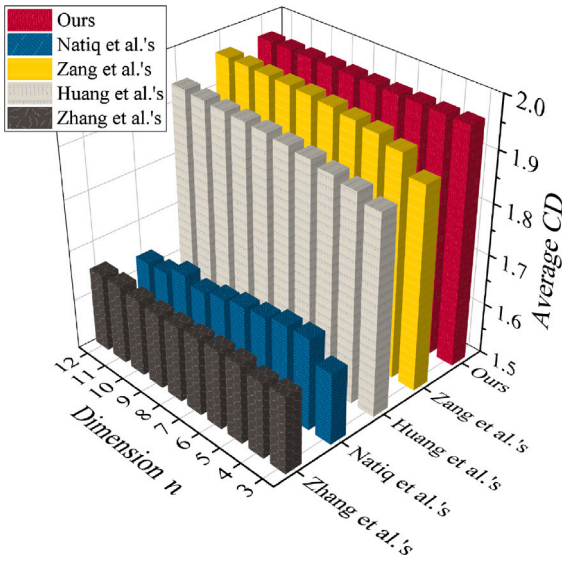

Fig. 5. The average CD of chaotic maps generated by each nD chaotic map generation method for investigated dimension $n \in \{3, 4, \ldots, 12\}$.

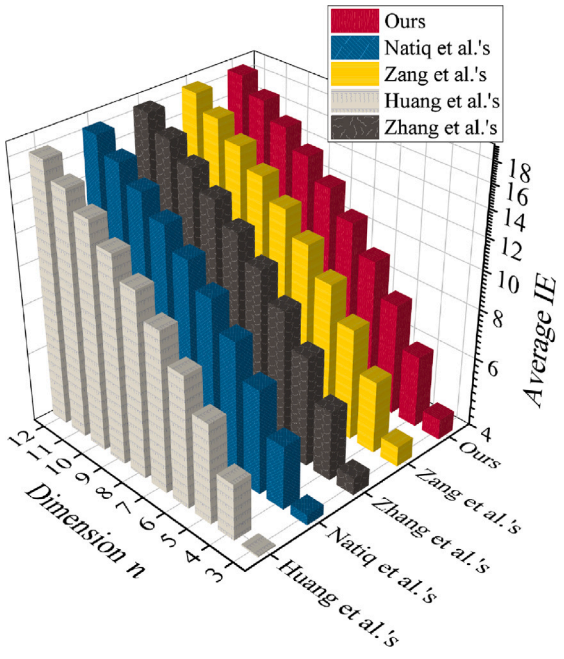

Fig. 6. The average IE of chaotic maps generated by each nD chaotic map generation method for investigated dimension $n \in \{3, 4, \ldots, 12\}$, with the number of divided parts $P = 3$.

compared to those generated by other methods. This emphasizes that the chaotic maps generated by our nD-CS yield uniformly distributed states, reflecting a high degree of uncertainty.

The other group analyzes the IEs against the number of divided parts $P = \{3, 5, \ldots, 23\}$ while fixing the investigated dimension $n = 3$. Therefore, for each generated 3D chaotic map, the initial state is set to $\mathbf{x}_0 = \{0.5\}^{n\times 1}$, and a total of P^{n+1} output states are produced to calculate the IE of the 3D chaotic map. Table 11 presents the average IEs of 100 3D chaotic maps generated by different methods. It can be seen that the 3D chaotic maps generated by our nD-CS exhibit the highest IE, which is also very close to the theoretical maximum IE value.

5. Conclusion

In this paper, we introduce a novel nD chaotic map generation method named the nD-CS. It is constructed from $n-1$ existing 1D seed maps and n linear functions. Each dimension of nD-CS incorporates the $n-1$ seed maps, a linear function, and a modular operation. Theoretical analysis proves that the proposed nD-CS exhibits chaotic behavior under the derived parameter-controlled criterion and consistently generates nD chaotic maps with n positive LEs. To demonstrate the effectiveness of nD-CS, we present three examples of 3D chaotic maps generated by nD-CS using the fraction, logistic, and sine maps as seed maps. These newly generated chaotic maps are evaluated using various indicators, including LE, SE, CD, IE, randomness test, trajectory, and fixed-point stability. The results demonstrate that they exhibit robust and complex dynamic behavior, a high level of irregularity, randomness, and spatial dimensionality. Furthermore, to comprehensively evaluate the performance of our nD-CS, we conduct vertical and horizontal comparisons of chaotic maps of different dimensions generated by nD-CS and other nD chaotic map generation methods. The analysis results reveal that the chaotic maps generated by nD-CS surpass those generated by the competing methods in various test indicators.

6. Future works

Our further work will explore the generation methods of nD chaotic maps in the complex field or investigate the study of chaotic systems in the complex domain. Extending the analysis to complex domains opens up new avenues for understanding the behavior and characteristics of chaos, potentially providing insights into phenomena not observable within the real domain alone.

CRediT authorship contribution statement

Zihua Wu: Writing – original draft, Validation, Methodology, Data curation, Conceptualization. **Yinxing Zhang:** Validation, Methodology, Investigation, Conceptualization. **Han Bao:** Validation, Methodology, Investigation, Formal analysis. **Rushi Lan:** Writing – review & editing, Validation, Supervision, Conceptualization. **Zhongyun Hua:** Writing – review & editing, Validation, Resources, Methodology, Funding acquisition.

Declaration of competing interest

The authors declare that they have no known competing financial interests or personal relationships that could have appeared to influence the work reported in this paper.

Data availability

Data will be made available on request.

Acknowledgments

This work was supported by the National Natural Science Foundation of China under Grants 62071142 and 62201094, by the Guangdong Basic and Applied Basic Research Foundation, China under Grant 2021A1515011406, and by the Shenzhen College Stability Support Plan, China under Grant GXWD20201230155427003-20200824210638001.

References

[1] Schuster HG, Just W. Deterministic chaos: an introduction. Hoboken, NJ, USA: John Wiley & Sons; 2006.
[2] Lorenz EN. Deterministic nonperiodic flow. J Atmos Sci 1963;20(2):130–41.
[3] Shen B-W, Pielke RA, Zeng X, Baik J-J, Faghih-Naini S, Cui J, et al. Is weather chaotic?: Coexistence of chaos and order within a generalized Lorenz model. Bull Am Meteorol Soc 2021;102(1):E148–58.
[4] Fruchart M, Hanai R, Littlewood PB, Vitelli V. Non-reciprocal phase transitions. Nature 2021;592(7854):363–9.
[5] Gumus OA, Selvam AG, Dhineshbabu R. Bifurcation analysis and chaos control of the population model with harvest. Int J Nonlinear Anal Appl 2022;13(1):115–25.
[6] Orlando G, Bufalo M, Stoop R. Financial markets' deterministic aspects modeled by a low-dimensional equation. Sci Rep 2022;12(1693):1–13.
[7] Li K, Bao H, Li H, Ma J, Hua Z, Bao B. Memristive Rulkov neuron model with magnetic induction effects. IEEE Trans Ind Inf 2022;18(3):1726–36.
[8] Bao H, Hua Z, Wang N, Zhu L, Chen M, Bao B. Initials-boosted coexisting chaos in a 2-D Sine map and its hardware implementation. IEEE Trans Ind Inf 2021;17(2):1132–40.
[9] Sriram G, Ali AMA, Natiq H, Ahmadi A, Rajagopal K, Jafari S. Dynamics of a novel chaotic map. J Comput Appl Math 2024;436(10). Art. no. 115453.
[10] Vaidyanathan S, Volos C. Advances and applications in chaotic systems. Berlin, Germany: Springer; 2016.
[11] Tsonis AA. Chaos: from theory to applications. New York, USA: Plenum Press; 1992.
[12] Wang X, Liu P. A new full chaos coupled mapping lattice and its application in privacy image encryption. IEEE Trans Circuits Syst I-Regul Pap 2022;69(3):1291–301.
[13] Li H, Hua Z, Bao H, Zhu L, Chen M, Bao B. Two-dimensional memristive hyperchaotic maps and application in secure communication. IEEE Trans Ind Electron 2021;68(10):9931–40.
[14] Murillo-Escobar D, Murillo-Escobar MÁ, Cruz-Hernández C, Arellano-Delgado A, López-Gutiérrez RM. Pseudorandom number generator based on novel 2D Hénon-Sine hyperchaotic map with microcontroller implementation. Nonlinear Dynam 2023;111(7):6773–89.
[15] Wang M, An M, He S, Zhang X, Ho-Ching Iu H, Li Z. Two-dimensional memristive hyperchaotic maps with different coupling frames and its hardware implementation. Chaos 2023;33(7). Art. no. 073129.
[16] Ali AMA, Sriram S, Natiq H, Ahmadi A, Rajagopal K, Jafari S. A novel multistable sinusoidal chaotic map with spectacular behaviors. Commun Theor Phys 2023;75(11). Art. no. 115001.
[17] Hilborn RC. Chaos and nonlinear dynamics: an introduction for scientists and engineers. Oxford, UK: Oxford Univ. Press; 2000.
[18] Luo Y, Yu J, Lai W, Liu L. A novel chaotic image encryption algorithm based on improved baker map and logistic map. Multimedia Tools Appl 2019;78:22023–43.
[19] Valle J, Machicao J, Bruno OM. Chaotical PRNG based on composition of logistic and tent maps using deep-zoom. Chaos Solitons Fractals 2022;161. Art. no. 112296.
[20] Talhaoui MZ, Wang X, Talhaoui A. A new one-dimensional chaotic map and its application in a novel permutation-less image encryption scheme. Visual Comput 2021;37:1757–68.
[21] Xu Q, Sun K, Cao C, Zhu C. A fast image encryption algorithm based on compressive sensing and hyperchaotic map. Opt Lasers Eng 2019;121:203–14.
[22] Mansouri A, Wang X. A novel one-dimensional sine powered chaotic map and its application in a new image encryption scheme. Inform Sci 2020;520:46–62.
[23] Ma C, Mou J, Li P, Liu T. Dynamic analysis of a new two-dimensional map in three forms: integer-order, fractional-order and improper fractional-order. Eur Phys J-Spec Top 2021;230(7):1945–57.
[24] Yan W, Dong W, Wang P, Wang Y, Xing Y, Ding Q. Discrete-time memristor model for enhancing chaotic complexity and application in secure communication. Entropy 2022;24(7). Art. no. 864.
[25] Peng Y, He S, Sun K. A higher dimensional chaotic map with discrete memristor. AEU-Int J Electron Commun 2021;129:1–7, Art. no. 153539.
[26] Zhang Y, Hua Z, Bao H, Huang H, Zhou Y. Generation of n-dimensional hyperchaotic maps using Gershgorin-type theorem and its application. IEEE Trans Syst Man Cybern-Syst 2023;53(10):6516–29.
[27] Sun C, Wang E, Zhao B. Image encryption scheme with compressed sensing based on a new six-dimensional non-degenerate discrete hyperchaotic system and plaintext-related scrambling. Entropy 2021;23(3). Art. no. 291.
[28] Zang H, Liu J, Li J. Construction of a class of high-dimensional discrete chaotic systems. Mathematics 2021;9(4). Art. no. 365.
[29] Zhang Y, Xiang H, Zhang S, Liu L. Construction of high-dimensional cyclic symmetric chaotic map with one-dimensional chaotic map and its security application. Multimedia Tools Appl 2022.
[30] Natiq H, Banerjee S, He S, Said M, Kilicman A. Designing an M-dimensional nonlinear model for producing hyperchaos. Chaos Solitons Fractals 2018;114:506–15.
[31] Huang L, Liu J, Xiang J, Zhang Z, Du X. A construction method of N-dimensional non-degenerate discrete memristive hyperchaotic map. Chaos Solitons Fractals 2022;160. Art. no. 112248.
[32] Geisel T, Fairen V. Statistical properties of chaos in Chebyshev maps. Phys Lett A 1984;105(6):263–6.
[33] De Oliveira JA, Papesso ER, Leonel ED. Relaxation to fixed points in the Logistic and Cubic maps: Analytical and numerical investigation. Entropy 2013;15(10):4310–8.
[34] Lu J, Wu X, Lü J, Kang L. A new discrete chaotic system with rational fraction and its dynamical behaviors. Chaos Solitons Fractals 2004;22:311–9.
[35] Herbadji D, Belmeguenai A, Derouiche N, Liu H. Colour image encryption scheme based on enhanced quadratic chaotic map. IET Image Process 2020;14(1):40–52.
[36] Hua Z, Zhou B, Zhou Y. Sine-transform-based chaotic system with FPGA implementation. IEEE Trans Ind Electron 2018;65(3):2557–66.
[37] Pikovsky A, Politi A. Lyapunov exponents: a tool to explore complex dynamics. Cambridge, UK: Cambridge Univ. Press; 2016.
[38] Schwengelbeck U, Faisal F. Definition of Lyapunov exponents and KS entropy in quantum dynamics. Phys Lett A 1995;199:281–6.
[39] Chen G, Lai D. Making a dynamical system chaotic: Feedback control of Lyapunov exponents for discrete-time dynamical systems. IEEE Trans Circuits Syst I 1997;44(3):250–3.
[40] Dieci L, Russell RD, Van Vleck ES. On the compuation of Lyapunov exponents for continuous dynamical systems. SIAM J Numer Anal 1997;34(1):402–23.
[41] Lu L-Z, Pearce CEM. Some new bounds for singular values and eigenvalues of matrix products. Ann Oper Res 2000;98:141–8.
[42] He J, Liu Y-M, Tian J-K, Ren Z-R. New inclusion sets for singular values. J Inequal Appl 2017;2017(64):1–8.
[43] Richman JS, Moorman JR. Physiological time-series analysis using approximate entropy and sample entropy. Am J Physiol-Heart Circulatory Physiol 2000;278(6):2039–49.
[44] Lacasa L, Gómez-Gardeñes J. Correlation dimension of complex networks. Phys Rev Lett 2013;110(16). Art. no. 168703.
[45] Shannon CE. A mathematical theory of communication. Bell Syst Tech J 1948;27(3):379–423.
[46] L'Ecuyer P, Simard R. TestU01: AC library for empirical testing of random number generators. ACM Trans Math Software 2007;33(4):1–40, Art. no. 22.
[47] Marsaglia G. DIEHARD: a battery of tests of randomness. Florida State University; 1996.
[48] Bassham III LE, Rukhin AL, Soto J, Nechvatal JR, Smid ME, Barker EB, et al. SP 800-22 Rev. 1a. A statistical test suite for random and pseudorandom number generators for cryptographic applications. Gaithersburg, MD, USA: Natl. Inst. Stand. Technol.; 2010.